New Coherent and Hybrid Detectors for Distributed MIMO Radar with Synchronization Errors

Cengcang Zeng, Fangzhou Wang, and Hongbin Li
ECE Department, Stevens Institute of Technology
Hoboken, NJ 07030, USA

Mark A. Govoni
Army Research Laboratory
Adelphi, MD 20783, USA

2021 IEEE Radar Conference (RadarConf21) | 978-1-7281-7609-3/20/$31.00 ©2021 IEEE | DOI: 10.1109/RadarConf2147009.2021.9455305

***Abstract*—We examine the impact of synchronization errors on target detection in distributed multi-input multi-output (MIMO) radar. The problem was initially considered in a recent work [1], which also introduced an approximate coherent detector (ACD). The ACD neglects the cross correlation of the radar waveforms, which may be significant in distributed MIMO radar. As the sensors are spatially distributed, the waveforms undergo different propagation delays and Doppler frequencies and thus may lose mutual orthogonality. The problem becomes more severe in the presence of synchronization errors. In this paper, we propose an improved coherent detector (CD) that takes into account the cross correlation in phase compensation and exploits different signal strength among different transmit-receive (TX-RX) paths. We also propose a new hybrid detector (HD) as a trade-off solution, in terms of detection performance and synchronization requirement, to bridge coherent detection and non-coherent detection. Numerical results are presented to illustrate the performance of existing and proposed detectors with or without synchronization errors.**

***Index Terms*—Distributed MIMO radar; non-orthogonal waveforms; asynchronous propagation; timing, frequency, and phase errors; target detection**

I. Introduction

A multi-input multi-output (MIMO) radar transmits multiple waveforms from its transmitters (TXs) to probe the environment. The receivers (RXs) employ a set of matched filters (MFs), one for each waveform, which are intended to unravel the radar echoes and separate the information carried by different waveforms. Most previous studies on distributed MIMO radar assume the transmit waveforms are orthogonal with zero cross-correlation across all time delays and Doppler frequencies and can be perfectly separated at each RX (e.g., [2]–[5]). However, in practice, it is impossible to maintain orthogonality with arbitrary delay and frequency shift [6], which means the MF output contains not only the filtered echo of the desired waveform, i.e., the *auto term*, but also the *cross term* from the undesired waveforms, thus resulting in non-ideal separation. The effects of cross terms were examined in [7], which treat them as deterministic unknowns, whereas in [8], [9], they were modeled as random quantities with an unknown covariance matrix. In either case, the waveform correlation, which is known, was not utilized.

This work was supported in part by the Army Research Office under Cooperative Agreement Number W911NF-19-2-0234 and the National Science Foundation under grant ECCS-1923739.

In distributed MIMO radar, sensors are spatially separated, driven by individual local clocks and oscillators, synchronization among TXs and RXs is non-trivial. Phase synchronization, which is essential in applications requiring coherent processing such as direction finding, were considered in several studies. Specifically, the phase identifiability problem in self-calibrating MIMO radar was discussed in [10]. Various phase synchronization schemes involving centralized or distributed processing were proposed in [11]. A number of works examined signal detection [12], direction finding [13], and beamforming [14] in the presence of phase errors when timing/frequency errors are negligible. While these studies underscore the importance of synchronization, joint investigations of the effects of timing, frequency, and phase errors, which are coupled with each other, on distributed MIMO radar are lacking.

We started to examine the impact of non-orthogonal waveforms and synchronization issues on distributed MIMO radar in [1]. We continue the investigation and present herein new advances in signal modeling and detection methods. Specifically, we develop a more general signal model which incorporates timing, frequency, and phase errors among RXs and TXs. To study the impacts of synchronization errors on target detection in distributed MIMO radar, we consider coherent and non-coherent target detection methods for distributed MIMO radar. We first briefly review a classical non-coherent detector (NCD) and a recently introduced approximate coherent detector (ACD) discussed in [1]. The ACD performs phase compensation only for the auto terms and neglect the cross terms. Moreover, it applies equal weights in combining different MF outputs, without accounting for their potential different SNRs associated with different TX-RX pairs. To address these problems, we propose an improved coherent detector (CD) that allows for cross terms and, moreover, exploits diversities in signal strength among different TX-RX paths. We also propose a new hybrid detector (HD) as a trade-off solution to bridge NCD and CD. HD coherently processes output samples of each MF and non-coherently integrates across different MFs. Since it requires phase coherence locally but not across spatially distributed antennas, HD bypasses the stringent phase synchronization requirement of CD and, meanwhile, enjoys additional coherent processing gain over NCD. Numerical results are presented to illustrate the performance of these non-coherent, coherent, and hybrid detectors with or without

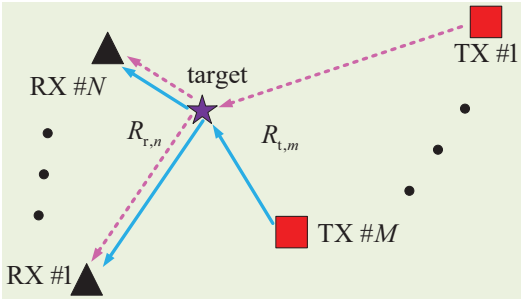

Fig. 1. Transmit and receive configuration of a distributed MIMO radar.

synchronization errors.

II. Signal Model

Consider a distributed MIMO radar system with M TXs and N RXs as shown in Fig. 1. The TXs employ pulsed transmission to probe an area of interest by using M waveforms. During a coherent processing interval, a succession of K periodic pulses are transmitted by each TX. Specifically, at the m-th TX, the transmitted pulses are given by

$$\tilde{s}_m(t) = b_m u_m(t) e^{\jmath[2\pi(\hat{f}_{\mathrm{c}}+\Delta^{\mathrm{c}}_{\mathrm{t},m})t+\phi_{\mathrm{t},m}]}, \tag{1}$$

where $u_m(t) = \sum_{k=0}^{K-1} p_m(t-kT_{\mathrm{s}})$ is the baseband transmitted signal, $p_m(t)$ is the complex envelope of a single pulse for TX m, T_{s} is the pulse repetition interval (PRI), b_m is the transmit amplitude, $\hat{f}_{\mathrm{c}}$ is the nominal carrier frequency, $\Delta^{\mathrm{c}}_{\mathrm{t},m}$ denotes the carrier frequency error introduced by the m-th TX, and $\phi_{\mathrm{t},m}$ is the carrier initial phase. The pulse waveform $p_m(t)$ has unit energy and is of the same duration T_{p} for all TXs. Therefore, $|b_m|^2$ denotes the energy transmitted in a single pulse.

Suppose there is a moving target at a distance $R_{\mathrm{t},m}$ to the m-th TX and a distance $R_{\mathrm{r},n}$ to the n-th RX. The signal $\tilde{s}_n(t)$ observed at the n-th RX consists of echoes from the target illuminated by M waveforms

$$\begin{aligned}\tilde{s}_n(t) = &\sum_{m=1}^{M} \alpha b_m \xi_{mn} u_m(t-\tau_{mn}) \\ &\times e^{\jmath 2\pi(\hat{f}_{\mathrm{c}}+\Delta^{\mathrm{c}}_{\mathrm{t},m}+\widetilde{f}_{mn})(t-\tau_{mn})} e^{\jmath\phi_{\mathrm{t},m}},\end{aligned} \tag{2}$$

where α is the target amplitude, $\tau_{mn} = (R_{\mathrm{t},m} + R_{\mathrm{r},n})/c$ is the (m,n)-th TX-RX propagation delay, and $\widetilde{f}_{mn}$ is the bistatic *target Doppler frequency* [4] observed by the n-th RX in response to the radar waveform transmitted from the m-th TX. In addition, ξ_{mn} is the channel coefficient associated with the (m,n)-th TX-RX pair [15]:

$$\xi_{mn} = \sqrt{\frac{G_{\mathrm{r},n} G_{\mathrm{t},m} \lambda^2}{(4\pi)^3 R^2_{\mathrm{t},m} R^2_{\mathrm{r},n}}}, \tag{3}$$

where λ is the wavelength of the signal and $G_{\mathrm{t},m}$ and $G_{\mathrm{r},n}$ are the m-th TX and, respectively, n-th RX antenna gain.

A local carrier $e^{\jmath[2\pi(\hat{f}_{\mathrm{c}}+\Delta^{\mathrm{c}}_{\mathrm{r},n})t+\phi_{\mathrm{r},n}]}$ is generated at the n-th RX for down conversion, where $\Delta^{\mathrm{c}}_{\mathrm{r},n}$ and $\phi_{\mathrm{r},n}$ denote the local carrier frequency error and initial phase, respectively. After down conversion, the baseband signal is

$$\begin{aligned}s_n(t) &= \sum_{m=1}^{M} \alpha b_m \xi_{mn} u_m(t-\tau_{mn}) e^{\jmath 2\pi(\hat{f}_{\mathrm{c}}+\Delta^{\mathrm{c}}_{\mathrm{t},m}+\widetilde{f}_{mn})(t-\tau_{mn})} \\ &\times e^{\jmath\phi_{\mathrm{t},n}} e^{-\jmath[2\pi(\hat{f}_{\mathrm{c}}+\Delta^{\mathrm{c}}_{\mathrm{r},n})t+\phi_{\mathrm{r},n}]} \\ &= \sum_{m=1}^{M} \alpha b_m \xi_{mn} u_m(t-\tau_{mn}) e^{\jmath\psi_{mn}} \\ &\times e^{-\jmath 2\pi(\hat{f}_{\mathrm{c}}+\Delta^{\mathrm{c}}_{\mathrm{r},n})\tau_{mn}} e^{\jmath 2\pi f_{mn}(t-\tau_{mn})},\end{aligned} \tag{4}$$

where $\psi_{mn} \triangleq \phi_{\mathrm{t},m} - \phi_{\mathrm{r},n}$ denotes the initial phase offset and $f_{mn} \triangleq \widetilde{f}_{mn} + \Delta^{\mathrm{c}}_{\mathrm{t},m} - \Delta^{\mathrm{c}}_{\mathrm{r},n}$ denotes the combined frequency offset between the m-th TX and n-th RX. A set of M matched filters (MFs), each matched to one of M waveforms, are used at the n-th RX. Each MF requires estimates of the target delay τ_{mn} and Doppler f_{mn} for compensation. In the following, we first consider the general case with possible synchronization errors, and then extend the result to the ideal case of no synchronization error, which is included as a benchmark for comparative studies.

At the n-th RX, $s_n(t)$ is convolved with M MFs, $g_m(t) = p^*_m(-t)e^{\jmath 2\pi(f_{mn}+\Delta^{\mathrm{f}}_{mn})t}$, $m = 1,\ldots,M$, where Δ^{f}_{mn} denotes the *frequency error* between the *effective Doppler frequency* f_{mn} and its estimate $\hat{f}_{mn}$. Let us define the *cross ambiguity function* (CAF) as

$$\chi_{m\bar{m}}(\nu, f) = \int p_m(\mu) p^*_{\bar{m}}(\mu-\nu) e^{\jmath 2\pi f\mu} d\mu. \tag{5}$$

Then, the output of the m-th MF at the n-th RX $x_{mn}(t)$ can be written as

$$\begin{aligned}x_{mn}(t) &= \sum_{\bar{m}=1}^{M} \alpha b_{\bar{m}} \xi_{\bar{m}n} e^{\jmath\psi_{\bar{m}n}} e^{-\jmath 2\pi(\hat{f}_{\mathrm{c}}+\Delta^{\mathrm{c}}_{\mathrm{r},n})\tau_{\bar{m}n}} e^{-\jmath 2\pi f_{\bar{m}n}\tau_{\bar{m}n}} \\ &\times e^{\jmath 2\pi(f_{mn}+\Delta^{\mathrm{f}}_{mn})t} \sum_{k=0}^{K-1} \int p_{\bar{m}}(\mu - kT_{\mathrm{s}} - \tau_{\bar{m}n}) \\ &\times p^*_m(\mu-t) e^{\jmath 2\pi(f_{\bar{m}n}-f_{mn}-\Delta^{\mathrm{f}}_{mn})\mu} d\mu \\ &= \sum_{\bar{m}=1}^{M} \alpha b_{\bar{m}} \xi_{\bar{m}n} e^{-\jmath 2\pi(\hat{f}_{\mathrm{c}}+\Delta^{\mathrm{c}}_{\mathrm{r},n})\tau_{\bar{m}n}} e^{\jmath 2\pi(f_{mn}+\Delta^{\mathrm{f}}_{mn})(t-\tau_{\bar{m}n})} \\ &\times e^{\jmath\psi_{\bar{m}n}} \sum_{k=0}^{K-1} \chi_{m\bar{m}}(t-\tau_{\bar{m}n}-kT_{\mathrm{s}}, f_{\bar{m}n}-f_{mn}-\Delta^{\mathrm{f}}_{mn}) \\ &\times e^{\jmath 2\pi kT_{\mathrm{s}}(f_{\bar{m}n}-f_{mn}-\Delta^{\mathrm{f}}_{mn})}.\end{aligned} \tag{6}$$

The continuous-time signal $x_{mn}(t)$ is sampled at the pulse rate, leading to K *slow-time samples* obtained at time instants $t = \tau_{mn} + \Delta^{\mathrm{t}}_{mn} + kT_{\mathrm{s}}$, $k = 0,\cdots,K-1$, where Δ^{t}_{mn} denotes the *timing error* between the true propagation delay τ_{mn} and

its estimate $\hat{\tau}_{mn}$. Then, the output samples can be written as

$$\begin{aligned} x_{mn}(k) &= x_{mn}(t)\Big|_{t=\tau_{mn}+\Delta^{\mathrm{t}}_{mn}+kT_{\mathrm{s}}} = \alpha b_m \xi_{mn} e^{\jmath 2\pi k T_{\mathrm{s}} f_{mn}} \\ &\times \chi_{mm}(\Delta^{\mathrm{t}}_{mn}, -\Delta^{\mathrm{f}}_{mn}) e^{-\jmath 2\pi(\hat{f}_{\mathrm{c}}+\Delta^{\mathrm{c}}_{\mathrm{r},n})\tau_{mn}} e^{\jmath 2\pi(f_{mn}+\Delta^{\mathrm{f}}_{mn})\Delta^{\mathrm{t}}_{mn}} \\ &\times e^{\jmath\psi_{mn}} + \sum_{\bar{m}\neq m} \alpha b_{\bar{m}} \xi_{\bar{m}n} e^{\jmath\psi_{\bar{m}n}} e^{-\jmath 2\pi(\hat{f}_{\mathrm{c}}+\Delta^{\mathrm{c}}_{\mathrm{r},n})\tau_{\bar{m}n}} e^{\jmath 2\pi k T_{\mathrm{s}} f_{\bar{m}n}} \\ &\times \chi_{m\bar{m}}(\tau_{mn}+\Delta^{\mathrm{t}}_{mn}-\tau_{\bar{m}n}, f_{\bar{m}n}-f_{mn}-\Delta^{\mathrm{f}}_{mn}) \\ &\times e^{\jmath 2\pi(f_{mn}+\Delta^{\mathrm{f}}_{mn})(\tau_{mn}+\Delta^{\mathrm{t}}_{mn}-\tau_{\bar{m}n})}, \qquad (7) \\ m &= 1,\ldots,M;\ n = 1,\ldots,N;\ k = 0,\ldots,K-1. \end{aligned}$$

Remark 1: It can be seen that the output sample $x_{mn}(k)$ consists of M components: the first term is the *auto term* between the m-th waveform and the m-th MF, and the other components represent the *cross terms* between the other $M-1$ waveforms and the m-th MF. The cross terms vanish when waveforms $p_m(t)$ are orthogonal to each other, which is a routine assumption in the MIMO literature. In practice, maintaining strict orthogonality across time and frequency in distributed MIMO radar with asynchronous propagation is infeasible [6]. With non-orthogonal waveforms or waveforms that are orthogonal only with zero delay/Doppler, cross terms are present as residuals, which may become non-negligible and need to be accounted for.

Next, we stack the K slow-time samples and form $\mathbf{x}_{mn} = [x_{mn}(0), \cdots, x_{mn}(K-1)]^T$, which can be expressed as

$$\mathbf{x}_{mn} = \alpha \mathbf{S}_n \boldsymbol{\mathcal{X}}_{mn} \mathbf{h}_{mn}, \qquad (8)$$

where the $K \times M$ Doppler steering matrix $\mathbf{S}_n$ is

$$\begin{aligned} \mathbf{S}_n &= [\mathbf{s}(f_{1n}), \cdots, \mathbf{s}(f_{Mn})], \qquad (9) \\ \mathbf{s}(f) &= [1, e^{\jmath 2\pi T_{\mathrm{s}} f}, \cdots, e^{\jmath 2\pi (K-1) T_{\mathrm{s}} f}]^T, \end{aligned}$$

the $M \times M$ ambiguity function matrix $\boldsymbol{\mathcal{X}}_{mn}$ is diagonal with diagonal elements given by

$$[\boldsymbol{\mathcal{X}}_{mn}]_{\bar{m}\bar{m}} = \chi_{m\bar{m}}(\tau_{mn}+\Delta^{\mathrm{t}}_{mn}-\tau_{\bar{m}n}, f_{\bar{m}n}-f_{mn}-\Delta^{\mathrm{f}}_{mn}), \qquad (10)$$

and the $\bar{m}$-th element of the $M \times 1$ channel vector $\mathbf{h}_{mn}$ is

$$\begin{aligned} [\mathbf{h}_{mn}]_{\bar{m}} &= b_{\bar{m}} \xi_{\bar{m}n} e^{\jmath\psi_{\bar{m}n}} e^{-\jmath 2\pi(\hat{f}_{\mathrm{c}}+\Delta^{\mathrm{c}}_{\mathrm{r},n})\tau_{\bar{m}n}} \\ &\times e^{\jmath 2\pi(f_{mn}+\Delta^{\mathrm{f}}_{mn})(\tau_{mn}+\Delta^{\mathrm{t}}_{mn}-\tau_{\bar{m}n})}. \qquad (11) \end{aligned}$$

III. Target Detection

Let $\mathbf{y}_{mn}$ denote the noise contaminated observation of $\mathbf{x}_{mn}$. The target detection problem is described by the following hypothesis testing:

$$\begin{aligned} \mathcal{H}_0 &: \mathbf{y}_{mn} = \mathbf{w}_{mn}, \\ \mathcal{H}_1 &: \mathbf{y}_{mn} = \alpha \mathbf{S}_n \boldsymbol{\mathcal{X}}_{mn} \mathbf{h}_{mn} + \mathbf{w}_{mn}, \qquad (12) \\ & \qquad m = 1, 2, \cdots, M,\ n = 1, 2, \cdots, N, \end{aligned}$$

where $\mathbf{w}_{mn}$ is the noise, assumed to be Gaussian distributed, $\mathbf{w}_{mn} \sim \mathcal{CN}(\mathbf{0}, \sigma^2_{mn}\mathbf{I})$. In the following, we consider target detection approaches for the general case, i.e., distributed MIMO radar with possible synchronization errors. For target detection, we discuss several detectors, including a conventional non-coherent detector (NCD) [3], an approximate coherent detector (ACD) [1], a coherent detector (CD), and a hybrid detector (HD). The latter two are new.

A. Non-Coherent Detector

A simple detector for the hypothesis testing (12) is based on non-coherent integration of the MF outputs [3]:

$$T_{\mathrm{NCD}} \triangleq \sum_{m=1}^{M} \sum_{n=1}^{N} \mathbf{y}^H_{mn} \mathbf{y}_{mn} \underset{\mathcal{H}_0}{\overset{\mathcal{H}_1}{\gtrless}} \gamma_{\mathrm{NCD}}, \qquad (13)$$

where γ_{NCD} is a threshold set for a given level of false alarm. It is clear that the above NCD is an energy detector.

B. Coherent Detectors

The above NCD does not require any phase synchronization. Improved detection performance can be achieved by exploiting phase information. One such detector, ACD, was introduced in [1], which performs phase compensation for the auto terms in the MF output (7). Specifically, let $\hat{\psi}_{mn}$, $\hat{\tau}_{mn}$, and $\hat{f}_{mn}$ denote estimates of the phase offset, delay, and Doppler frequency. The ACD is given by

$$T_{\mathrm{ACD}} = \left| \sum_{m=1}^{M} \sum_{n=1}^{N} \sum_{k=0}^{K-1} e^{-\jmath\hat{\theta}_{mnk}} y_{mn}(k) \right|^2 \underset{\mathcal{H}_0}{\overset{\mathcal{H}_1}{\gtrless}} \gamma_{\mathrm{ACD}}, \qquad (14)$$

where γ_{ACD} is the threshold, $y_{mn}(k)$ denotes the k-th element of $\mathbf{y}_{mn}$ and

$$\begin{aligned} \hat{\theta}_{mnk} &= \hat{\psi}_{mn} - 2\pi \hat{f}_{\mathrm{c}} \hat{\tau}_{mn} + 2\pi k T_{\mathrm{s}} \hat{f}_{mn}, \qquad (15) \\ \hat{\psi}_{mn} &\triangleq \psi_{mn} + \Delta^{\mathrm{p}}_{mn}, \qquad (16) \\ \hat{\tau}_{mn} &\triangleq \tau_{mn} + \Delta^{\mathrm{t}}_{mn}, \qquad (17) \\ \hat{f}_{mn} &\triangleq f_{mn} + \Delta^{\mathrm{f}}_{mn}, \qquad (18) \end{aligned}$$

where Δ^{p}_{mn}, Δ^{t}_{mn}, and Δ^{f}_{mn} denote the phase, timing, and Doppler errors.

Albeit simple, the ACD has two limitations. First, it performs phase compensation only for the auto-term, while neglecting the cross terms in (7), which is non-negligible when the waveforms are not orthogonal. Second, it applies equal weights in combining the outputs from different MFs, which is suboptimal since the TX-RX propagation paths associated with different MFs are different with potentially different SNRs.

To address these limitations, an improved CD can be derived by using a generalized likelihood ratio test (GLRT) approach to solve the hypothesis testing problem (12). Specifically, we first obtain the maximum likelihood estimate (MLE) of the target amplitude α, and then use the MLE in the likelihood ratio of (12). The resulting CD detector is summarized as follows. Let $\hat{\mathbf{S}}_n$, $\hat{\boldsymbol{\mathcal{X}}}_{mn}$, and $\hat{\mathbf{h}}_{mn}$ be formed as in (9)-(11), by using prior estimates of the phase, delay, and Doppler frequency:

$$\begin{aligned} \hat{\mathbf{S}}_n &= [\mathbf{s}(\hat{f}_{1n}), \cdots, \mathbf{s}(\hat{f}_{Mn})], \qquad (19) \\ [\hat{\boldsymbol{\mathcal{X}}}_{mn}]_{\bar{m}\bar{m}} &= \chi_{m\bar{m}}(\hat{\tau}_{mn}-\hat{\tau}_{\bar{m}n}, \hat{f}_{\bar{m}n}-\hat{f}_{mn}), \qquad (20) \\ [\hat{\mathbf{h}}_{mn}]_{\bar{m}} &= b_{\bar{m}} \xi_{\bar{m}n} e^{\jmath\hat{\psi}_{\bar{m}n}} e^{-\jmath 2\pi \hat{f}_{\mathrm{c}} \hat{\tau}_{\bar{m}n}} e^{\jmath 2\pi \hat{f}_{mn}(\hat{\tau}_{mn}-\hat{\tau}_{\bar{m}n})}. \qquad (21) \end{aligned}$$

Then, the new CD is given by

$$T_{\text{CD}} = \left| \sum_{m=1}^{M} \sum_{n=1}^{N} (\hat{\mathbf{S}}_n \hat{\boldsymbol{\mathcal{X}}}_{mn} \hat{\mathbf{h}}_{mn})^H \mathbf{y}_{mn} \right|^2 \underset{\mathcal{H}_0}{\overset{\mathcal{H}_1}{\gtrless}} \gamma_{\text{CD}}, \tag{22}$$

where γ_{CD} denotes the test threshold. It can be seen that the CD sequentially performs Doppler filtering by $\hat{\mathbf{S}}_n$, joint phase compensation and amplitude weighting by $\hat{\boldsymbol{\mathcal{X}}}_{mn}$ and $\hat{\mathbf{h}}_{mn}$, followed by coherent integration across antennas.

C. Hybrid Detector

The above CD requires the knowledge of the phases, the CAFs of all waveforms, and the channel coefficients $\boldsymbol{\xi}_{mn}$. Although achieving the best performance with ideal knowledge, CD is sensitive to knowledge/estimation errors. Another new HD detector can be obtained by using the GLRT approach. Specifically, the idea is to treat $\alpha \mathbf{h}_{mn}$ as an unstructured $M \times 1$ unknown vector. We can first obtain the MLE $\widehat{\alpha \mathbf{h}}_{mn}$ of this vector, and then use the MLE in the likelihood ratio of (12). The resulting HD is given by

$$T_{\text{HD}} = \sum_{m=1}^{M} \sum_{n=1}^{N} \|\hat{\mathbf{S}}_n (\hat{\mathbf{S}}_n^H \hat{\mathbf{S}}_n)^{-1} \hat{\mathbf{S}}_n^H \mathbf{y}_{mn}\|^2 \underset{\mathcal{H}_0}{\overset{\mathcal{H}_1}{\gtrless}} \gamma_{\text{HD}}. \tag{23}$$

Clearly, HD projects $\mathbf{y}_{mn}$ onto the subspace spanned by the Doppler steering vectors $\hat{\mathbf{S}}_n$, which is coherent processing of the signal observed at the (m,n)-th MF, followed by non-coherent integration across different RXs and TXs. Hence, it is a *hybrid* detector. Note that HD requires phase coherent only locally, i.e., within the output of each MF, but not across spatially distributed antennas. As such, HD detector bypasses the more stringent coherence requirement of CD, while it can still benefit from local coherent integration and achieve considerable improvement over the NCD, i.e., it offers a compromise between CD and NCD.

IV. Simulation Results

Simulation results are presented to compare the NCD [3], ACD [1], along with the proposed CD and HD, for target detection in distributed MIMO radar. The SNR of the (m,n)-th propagation path, which is measured at the n-th RX matched to the m-th TX waveform, is defined as

$$\text{SNR}_{mn} = \frac{|b_m \xi_{mn}|^2 \mathbb{E}\{|\alpha|^2\}}{\sigma_{mn}^2}, \tag{24}$$

where the noise variance is chosen as $\sigma_{mn}^2 = 1$ and $\mathbb{E}\{\cdot\}$ represents the statistical expectation. We consider a Swerling I target model, where the target amplitude $\alpha \sim \mathcal{CN}(0, \sigma^2)$ is randomly generated from trial to trial but remains fixed within a coherent processing interval (CPI) in Monte Carlo simulations. We assume identical SNR for all paths, i.e., $\text{SNR}_{mn} = \text{SNR}$, $\forall m,n$, except in the first example (Fig. 2). The simulation scenarios involve a distributed MIMO radar with $M = 2$ TXs and $N = 1$ RX. The propagation delays are $\tau_{11} = 0.61\tau$ and $\tau_{21} = 0.1\tau$ unless otherwise stated, where $\tau = 10^{-5}$ s is the pulse duration. The pulse repetition frequency (PRF) is 500 Hz, the carrier frequency is 3 GHz

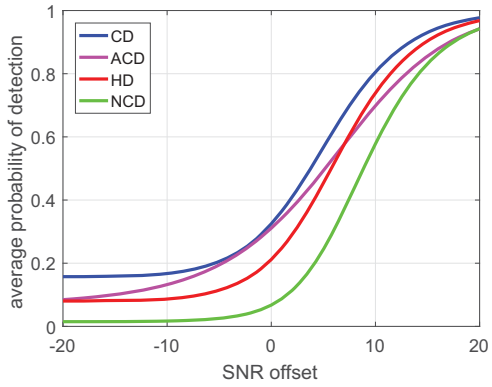

Fig. 2. $\bar{P}_d$ of distributed MIMO radar versus SNR offset $\text{SNR}_{21} - \text{SNR}_{11}$, where $\text{SNR}_{11} = 0$ dB.

and the waveform bandwidth is 1MHz. The target Doppler frequencies are $f_{11} = 200$ Hz and $f_{21} = 190$ Hz, unless otherwise stated, and the number of pulses within a CPI is $K = 12$. The phases are $\psi_{11} = 0.1\pi$ and $\psi_{21} = 0.3\pi$ unless otherwise stated and the probability of false alarm is $P_f = 10^{-4}$.

The radar waveforms are *single-band* linear frequency modulation (LFM) waveforms or chirps with overlapping instantaneous frequency [1]. For $M = 2$, we employ an up chirp

$$p_{\text{u}}(t) = \frac{1}{\sqrt{\tau}} e^{\jmath(\pi\beta t^2/\tau + \kappa\pi\beta t)}, \; 0 \le t < \tau, \tag{25}$$

and a down chirp

$$p_{\text{d}}(t) = \frac{1}{\sqrt{\tau}} e^{\jmath(-\pi\beta t^2/\tau + 2\pi\beta t + \kappa\pi\beta t)}, \; 0 \le t \le \tau, \tag{26}$$

where κ is a constant that controls the center frequency of the chirps and β is the bandwidth of the waveform. The ambiguity functions of the single-band chirps can be found in [1], which shows that the waveforms are *non-orthogonal* with high cross ambiguity.

First, we test the effect of unequal channel strength, where the two propagation paths from the TXs to the RX have different SNR. In particular, we fix $\text{SNR}_{11} = 0$ dB while varying SNR_{21}. Fig. 2 depicts the average probability of detection $\bar{P}_d$ versus SNR_{21}. It shows that CD outperforms both ACD and HD, where the benefit comes from the amplitude weighting and, respectively, fully coherent processing employed by CD. In addition, both HD and ACD outperforms the completely non-coherent NCD, and the relative performance between HD and ACD depends on the SNR offset.

Next we evaluate the effects of synchronization errors, including timing, phase, and Doppler frequency errors, on detection performance. Fig. 3 depicts the performance of CD, HD, and NCD under various timing conditions. It is seen that in general, as the timing error increases, the performance of all 3 detectors degrades. This is because a larger timing error implies the sampling location is further away from the peak of the auto ambiguity function, which results in a higher loss of the energy of the desired auto term and the associated SNR. It was observed in [1], if the timing error is much smaller than

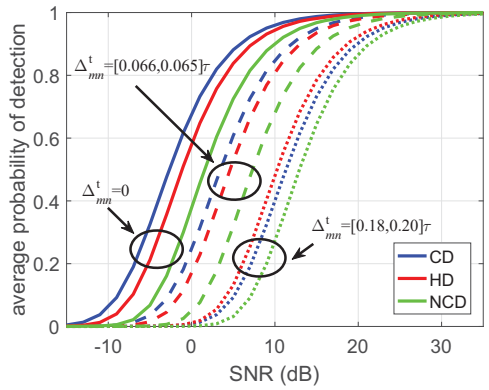

Fig. 3. $\bar{P}_d$ of distributed MIMO radar versus SNR without timing errors ($\Delta^{\mathrm{t}}_{mn} = 0$) or with two sets of timing errors.

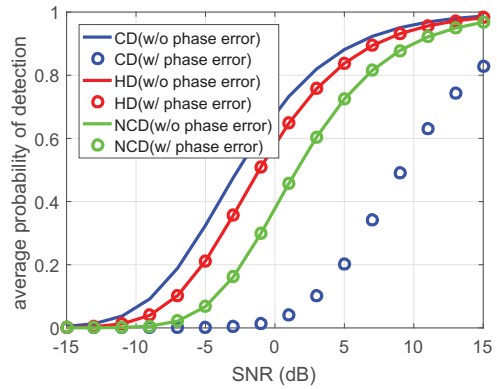

Fig. 4. $\bar{P}_d$ of distributed MIMO radar versus SNR without phase error ($\Delta^{\mathrm{p}}_{mn} = 0$) or with phase errors ($\Delta^{\mathrm{p}}_{11} = 0.023\pi$ and $\Delta^{\mathrm{p}}_{21} = 0.76\pi$).

the reciprocal of the waveform bandwidth but still significant relative to the carrier period so that the SNR loss is negligible, then it will only impact coherent detectors such as ACD as the timing-error-induced phase error may not be negligible. The observation applies to CD as well. For space limitation, we do not duplicate the result here.

The impact of phase error is shown in Fig. 4. It is observed that the phase error only affects CD, which is because the implementation of HD and NCD does not require any knowledge of the phase while the CD requires it for coherent integration across antennas. On the other hand, Fig. 5 shows the impact of Doppler frequency error. It is seen that Doppler frequency error degrades the performance of both CD and HD but not that of NCD.

V. Conclusions

We examined the impact of synchronization errors on target detection in distributed MIMO radar. Our main contributions include the general asynchronous signal model for distributed MIMO radar, the new CD and HD detectors. Our results indicate that synchronization errors in timing, frequency, and phase have different impacts on different detectors. Specifically, NCD and HD are immune from phase errors, which affect only coherent detectors ACD and CD. On the other hand, the frequency errors will affect all but NCD. Finally,

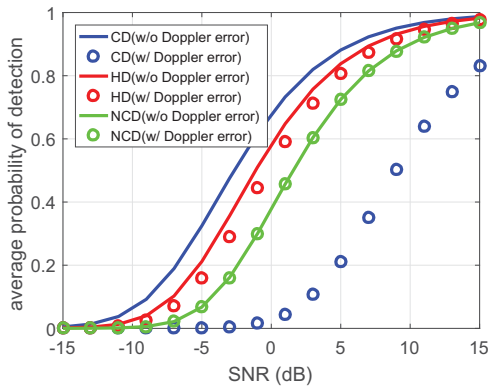

Fig. 5. $\bar{P}_d$ of distributed MIMO radar versus SNR without Doppler frequency errors ($\Delta^{\mathrm{f}}_{mn} = 0$) or with Doppler frequency errors ($\Delta^{\mathrm{f}}_{11} = -10$ Hz and $\Delta^{\mathrm{f}}_{21} = 25$ Hz).

all detectors are affected by timing errors, which cause the MF output to be sampled off the peak location of the auto ambiguity function, thus resulting in a loss in the SNR.

References

[1] F. Wang, C. Zeng, H. Li, and M. A. Govoni, "Detection performance of distributed MIMO radar with asynchronous propagation and timing/phase errors," in *2020 IEEE International Radar Conference (RADAR)*, April 2020, pp. 13–18.

[2] J. Li and P. Stoica, "MIMO radar with colocated antennas," *IEEE Signal Processing Magazine*, vol. 24, no. 5, pp. 106–114, 2007.

[3] A. M. Haimovich, R. S. Blum, and L. J. Cimini, "MIMO radar with widely separated antennas," *IEEE Signal Processing Magazine*, vol. 25, no. 1, pp. 116–129, 2008.

[4] P. Wang, H. Li, and B. Himed, "Moving target detection using distributed MIMO radar in clutter with nonhomogeneous power," *IEEE Transactions on Signal Processing*, vol. 59, no. 10, pp. 4809–4820, 2011.

[5] M. A. Govoni, R. Elwell, T. Dogaru, and D. Liao, "A practical look at target detection using MIMO radar," in *SPIE Defense, Security, and Sensing Conference*, vol. 9461, May 2015, pp. 228–238.

[6] Y. I. Abramovich and G. J. Frazer, "Bounds on the volume and height distributions for the MIMO radar ambiguity function," *IEEE Signal Processing Letters*, vol. 15, pp. 505–508, 2008.

[7] M. Akcakaya and A. Nehorai, "MIMO radar sensitivity analysis for target detection," *IEEE Transactions on Signal Processing*, vol. 59, no. 7, pp. 3241–3250, 2011.

[8] P. Wang, H. Li, and B. Himed, "Moving target detection for distributed MIMO radar with imperfect waveform separation," in *2013 IEEE Radar Conference (RadarCon13)*, 2013, pp. 1–5.

[9] P. Wang and H. Li, "Target detection with imperfect waveform separation in distributed MIMO radar," *IEEE Transactions on Signal Processing*, vol. 68, pp. 793–807, 2020.

[10] P. Sun, J. Tang, S. Wan, and N. Zhang, "Identifiability analysis of local oscillator phase self-calibration based on hybrid Cramér-Rao Bound in MIMO radar," *IEEE Transactions on Signal Processing*, vol. 62, no. 22, pp. 6016–6031, 2014.

[11] Y. Yang and R. S. Blum, "Phase synchronization for coherent MIMO radar: Algorithms and their analysis," *IEEE Transactions on Signal Processing*, vol. 59, no. 11, pp. 5538–5557, 2011.

[12] M. Akakaya and A. Nehorai, "MIMO radar detection and adaptive design under a phase synchronization mismatch," *IEEE Transactions on Signal Processing*, vol. 58, no. 10, pp. 4994–5005, 2010.

[13] Q. He and R. S. Blum, "Cramér-Rao Bound for MIMO radar target localization with phase errors," *IEEE Signal Processing Letters*, vol. 17, no. 1, pp. 83–86, Jan 2010.

[14] W. Zhang and S. A. Vorobyov, "Joint robust transmit/receive adaptive beamforming for MIMO radar using probability-constrained optimization," *IEEE Signal Processing Letters*, vol. 23, no. 1, pp. 112–116, 2016.

[15] M. A. Richards, *Fundamentals of Radar Signal Processing*. New York, NY, USA: McGraw-Hill, 2005.